Characteristics of iodine-123 IQ-SPECT/CT imaging compared with conventional SPECT/CT.

著者	Shibutani Takayuki, Onoguchi Masahisa, Yoneyama Hiroto, Konishi Takahiro, Matsuo Shinro, Nakajima Kenichi
著者別表示	澁谷 孝行, 松尾 信郎 , 中嶋 憲一
journal or publication title	Annals of Nuclear Medicine
volume	33
number	2
page range	103-111
year	2019-02-25
URL	http://doi.org/10.24517/00053810

doi: 10.1007/s12149-018-1310-8

Original Article

Characteristics of Iodine-123 IQ-SPECT/CT imaging compared with conventional SPECT/CT

Takayuki Shibutani[1)] iwsb03100621@staff.kanazawa-u.ac.jp
Masahisa Onoguchi[1)] onoguchi@staff.kanazawa-u.ac.jp
Hiroto Yoneyama[2)] kizu@cf6.so-net.ne.jp
Takahiro Konishi[2)] knstkhr.1985@gmail.com
Shinro Matsuo[3)] smatsuo@nmd.m.kanazawa-u.ac.jp
Kenichi Nakajima[3)] nakajima@med.kanazawa-u.ac.jp

1) Department of Quantum Medical Technology, Institute of Medical, Pharmaceutical and Health Sciences, Kanazawa University, Kanazawa, Japan
2) Department of Radiological Technology, Kanazawa University Hospital, Kanazawa, Japan
3) Department of Nuclear Medicine, Kanazawa University Hospital, Kanazawa, Japan

Abstract

Objectives Although the utility of IQ-SPECT imaging using ^{99m}Tc and ^{201}Tl myocardial perfusion SPECT has been reported, ^{123}I-labeled myocardial SPECT has not been fully evaluated. We determined the characteristics and utility of ^{123}I IQ-SPECT imaging compared with conventional SPECT (C-SPECT).

Methods Two myocardial phantom patterns were used to simulate normal myocardium and myocardial infarction. SPECT acquisition was performed using a hybrid dual-head SPECT/CT system equipped with a SMARTZOOM collimator for IQ-SPECT or a low-medium energy general purpose collimator for C-SPECT. Projection data were reconstructed using ordered subset expectation maximization with depth-dependent 3-dimensional resolution recovery for C-SPECT and ordered subset conjugate gradient minimizer method for IQ-SPECT. Three types of myocardial image were created; namely, no correction (NC), with attenuation correction (AC), and with both attenuation and scatter corrections (ACSC). Five observers visually scored the homogeneity of normal myocardium and defect severity of the myocardium with inferior defects by a five-point scale: homogeneity scores (5 = homogeneous to 1 = inhomogeneous) and defect scores (5 = excellent to 1= poor). We also created a 17-segment polar map and quantitatively assessed segmental %uptake using a myocardial phantom with normal findings and defects.

Results The average visual homogeneity scores of the IQ-SPECT with NC and ACSC were significantly higher than that of C-SPECT, whereas the average visual defect scores of IQ-SPECT with AC and ACSC were significantly lower. The %uptake of all segments for IQ-SPECT with NC was significantly higher than that of C-SPECT. Furthermore, the subtraction of %uptake for C-SPECT and IQ-SPECT was the largest in inferior wall, which was approximately 10.1%, 14.7% and 14.4% for NC, AC and ACSC, respectively. The median % uptake values of the inferior wall with defect areas for C-

SPECT and IQ-SPECT were 46.9% and 50.7% with NC, 59.8% and 69.2% with AC, and 54.7% and 66.5% with ACSC, respectively

Conclusion ^{123}I IQ-SPECT imaging significantly improved the attenuation artifact compared with C-SPECT imaging. Although the defect detectability of IQ-SPECT was inferior to that of C-SPECT, ^{123}I IQ-SPECT images with NC and ACSC met the criteria for defect detectability. Use of ^{123}I IQ-SPECT is suitable for routine examinations.

Keywords IQ-SPECT ・ multi-focus collimator ・ Iodine-123 ・ short acquisition ・OSCGM

Introduction

Nuclear cardiac imaging with Iodine-123 (^{123}I) radiopharmaceuticals including meta-iodobenzylguandine (MIBG) and beta-methyl-p-iodophenylpentadecanoic acid (BMIPP) is used in Japan [1]. ^{123}I-MIBG imaging reflects the distribution of cardiac sympathetic nerve terminals, and is widely used for the diagnosis of heart failure [2 – 6], Parkinson's disease [7, 8] and dementia with Lewy bodies [9 – 13]. ^{123}I-BMIPP imaging reflects the distribution of fatty acid metabolism, and is useful for the diagnosis of unstable angina, vasospastic angina and Takotsubo cardiomyopathy [14 – 16]. However, ^{123}I myocardial imaging using a parallel-hole collimator with an anger-type single photon emission computed tomography – computed tomography (SPECT-CT) (conventional SPECT [C-SPECT]) system is routinely conducted in a supine position with the arms raised above the head to avoid increased attenuation and to minimize the distance between the thorax and camera. In addition, C-SPECT image acquisition requires a long examination time of 15-20 min. In clinical examination, this is highly uncomfortable and sometimes causes deterioration of image quality due to patient motion [17 – 18]. To resolve these problems, short-time acquisition technology has been proposed [19 – 22]. Recently, the IQ-SPECT imaging system has been introduced as a method for short-term acquisition of myocardial SPECT images, which has been enabled by three technologies: a multifocal shaped SMARTZOOM collimator (SZC), rotational orbit around the center of the heart, and image reconstruction using the ordered subset conjugate gradient minimizer (OSCGM) method [23, 24]. The utility of the IQ-SPECT system using technetium-99m (^{99m}Tc) and thallium-201 (^{201}Tl) myocardial perfusion SPECT has been reported in technological and clinical studies [25 – 33]. Although simultaneous ^{99m}Tc and ^{123}I dual-radionuclide myocardial SPECT has been evaluated using Monte Carlo simulations and phantom experiment [34], myocardial SPECT with a single ^{123}I-labeled radiopharmaceutical has not been fully evaluated. The objective of this study

was to determine the characteristics and utility of IQ-SPECT imaging with a ^{123}I agent in comparison to those of C-SPECT.

Material and methods

Phantom designs

An anthropomorphic phantom featuring inserts to simulate the lungs, liver, left ventricular (LV) wall and LV chamber (Data spectrum Corp., Durham, NC, USA) was used in this study. Two myocardial phantoms that simulate normal myocardium and myocardial infarction were created. The myocardial defect was filled with nonradioactive water to simulate a transmural defect with rectangular shapes (major axis: 30mm, minor axis: 20 mm) located in the mid to basal inferior position in the LV wall (Fig.1). The lung inserts were filled with styrofoam beads. The radioactive concentration of the ^{123}I solution was 143 kBq/mL for the myocardium, 77 kBq/mL for the liver and 9 kBq/mL for both the LV chamber and the mediastinum. The radioactive concentration ratio of the myocardium, liver, LV chamber and mediastinum was 14, 8, 1 and 1, respectively, as determined previously [35].

Acquisition protocols and image reconstruction parameters

A hybrid dual-head SPECT/CT system (Symbia T6, Siemens, Tokyo, Japan) equipped with an SZC for IQ-SPECT or a low-medium energy general purpose collimator (LMEGP) for C-SPECT was used. The main photo-peak energy window of 15% width centered on 159 keV and a contiguous scatter window of 15% of the 159 keV photo-peak were set as the upper and lower parameters of the main window. The acquisition parameters for C-SPECT were a 64×64 matrix size, 6.6 mm pixel size, zoom factor of 1.45, total of 60 projections, circular orbit (radius of rotation: 24 cm) of 360° and center of rotation of 24 cm. For each detector, thirty views were acquired, and the total acquisition time was 20 min (35 sec/view). Meanwhile, the acquisition conditions of IQ-SPECT were a 128×128 matrix size, 4.8 mm pixel size and zoom factor of one. The spatial resolution progressively increased from the camera surface to the

cardiac sweet-spot at 28 cm, which was set as the center of rotation for this study, thereby keeping the LV phantom at the highest magnification throughout the acquisition. A scan acquired from the right anterior oblique 59° to the left posterior oblique 59° with 6° angular steps was used for each of the camera heads. For each detector, seventeen views were acquired, and the total acquisition time was 5 min 23 sec (14 sec/view). The CT scanning parameters for both C-SPECT and IQ-SPECT were a slice thickness of 5 mm, tube voltage of 130 kVp, tube current–time of 20 mAs, rotation speed of 0.6 sec/rotation, and scan pitch of 0.8 mm.

The projection data for C-SPECT were reconstructed using ordered subset expectation maximization with depth-dependent 3-dimensional resolution recovery (Flash3D; Siemens Healthcare, Erlangen, Germany) [36, 37]. Subsets and iterations were 10 and 12, respectively. A Gaussian filter (full width at half maximum [FWHM] = 13.2 mm) was used as a post-filter. We determined the image reconstruction parameter using Flash3D technology with reference to a previous study [37]. The IQ-SPECT images were reconstructed using the OSCGM method [23, 24]. Subsets and iterations were 3 and 10, respectively. A Gaussian filter (FWHM 9.6 mm) was used as a post-filter. The triple energy window method was used for scatter correction (SC). The attenuation correction (AC) was applied using a patient-dedicated low-dose CT-derived μ map. The AC and SC were performed for both C-SPECT and IQ-SPECT.

Three types of myocardial images were created; namely, (1) no correction (NC) without SC and AC, (2) with AC, and (3) with both AC and SC (ACSC).

Data analysis

Five nuclear cardiology experts each with >15 years' clinical experience visually scored the homogeneity of the normal myocardium on a five-point scale (5 = definite homogeneity, 4 = probable homogeneity, 3 = equivocal, 2 = probable inhomogeneity, and 1 = definite inhomogeneity) using the reconstructed C-SPECT and IQ-SPECT images. Moreover, the detectability

of defects in the myocardium with inferior wall defects was also assessed using a five-point scale (5 = excellent, 4 = good, 3 = equivocal, 2 = bad, 1 = poor). Visual homogeneity and defects were confirmed by a score of >4 points. We created a 17-segment polar map [16] and quantitatively assessed the %uptake of each segment for the myocardial phantom with normal and inferior wall defects. In addition, the difference of the %uptake in each segment between C-SPECT and IQ-SPECT imaging was compared using the subtraction polar map, and subsequently, the difference between C-SPECT and IQ-SPECT imaging was evaluated by subtraction of the average %uptake value. Furthermore, the variation of %uptake in the normal myocardium was evaluated using the coefficient of variance (CV) percentage. Comparison of the myocardium with inferior wall defects by C-SPECT and IQ-SPECT imaging was also evaluated by the average %uptake values of the mid and basal inferior walls. In addition, the extent of myocardial defects was evaluated by the average value of the circumferential count profiles of three slices for short axial image, which was quantitatively analyzed by the number of radians in the three count profiles of <60% for NC, 70% for AC, and ACSC of maximal counts, as described previously [29, 32, 38]. We also provided a clinical case demonstration to validate the utility of our study, which was approved by the institutional ethics committee of our institution.

Statistical analysis was performed using a statistical package for social science (SPSS) software (version 21 for Windows, SPSS Inc., Chicago, IL). The visual score of myocardium with normal and inferior wall defects was evaluated by Mann Whitney-u test. The %uptake of each segment with normal myocardium was examined by paired t-test. All p values less than 0.05 were considered to be statistically significant.

Results

The average visual homogeneity scores of the C-SPECT and IQ-SPECT normal myocardial images were 2.3 ± 0.7 and 3.3 ± 0.9 with NC, 4.2 ± 0.4 and 4.5 ± 0.5 with AC, and 3.3 ± 0.5 and 4.2 ± 0.6 with ACSC, respectively (Fig.2).

The IQ-SPECT score with NC and ACSC was significantly higher than that of C-SPECT (p= 0.01 with NC and p= 0.005 with ACSC). Furthermore, the AC image scores were significantly higher than the NC image scores (p< 0.001 with C-SPECT, p= 0.002 with IQ-SPECT), whereas the C-SPECT with ACSC score was significantly lower than the C-SPECT with AC score (p= 0.001). The average visual defect scores for C-SPECT and IQ-SPECT were 4.9 ± 0.3 and 4.6 ± 0.5 with NC, 4.6 ± 0.5 and 2.8 ± 0.8 with AC and 4.9 ± 0.3 and 4.0 ± 0.5 with ACSC, respectively (Fig.3). The C-SPECT with AC and ACSC scores were significantly higher than those of IQ-SPECT (p< 0.001 with AC, p= 0.001 with ACSC). The IQ-SPECT with AC image scores was significantly lower than the IQ-SPECT with NC image score (p< 0.001). However, the ACSC images achieved significantly higher visual defect scores than did the AC images (p= 0.002).

The average %uptake values of C-SPECT and IQ-SPECT for all segments were 73.8 ± 9.5% and 76.4 ± 8.0% with NC, 86.5 ± 3.6% and 87.6 ± 3.9% with AC and 83.6 ± 4.4% and 84.1 ± 4% with ACSC, respectively (Fig.4). The %uptake of IQ-SPECT with NC was significantly higher than that of C-SPECT (p= 0.015). Furthermore, the difference in the %uptake between C-SPECT and IQ-SPECT was the largest in the inferior wall, which was approximately 13% among the correction methods. The %CVs of C-SPECT and IQ-SPECT were 12.9% and 10.4% with NC, 4.2% and 4.4% with AC, and 5.3% and 4.8 with ACSC, respectively. The %CV of IQ-SPECT with NC was lower than that of C-SPECT with NC.

The median % uptake values of the inferior wall with defect areas (segments 4 and 10) between C-SPECT and IQ-SPECT were 46.9% and 50.7% with NC, 59.8% and 69.2% with AC, and 54.7% and 66.5% with ACSC, respectively (Fig.5). Moreover, IQ-SPECT showed a 4 – 11% higher %uptake value than did the C-SPECT. The radians of the inferior defects for C-SPECT and IQ-SPECT were 1.87 and 1.47 for NC, 1.47 and 0.24 for AC, and 1.66 and 0.76 for ACSC, respectively (Fig.6). IQ-SPECT with NC, AC and ACSC had a lower radian value and higher %uptake than did C-SPECT. Figure 7 provides the

short axis images with NC, AC, and ACSC of C-SPECT and IQ-SPECT for the myocardial phantom with normal findings and the inferior wall defects.

Normal IQ-SPECT distribution in a clinical sample

A 54-year-old woman with parkinsonism with akinesia and left-hand tremor was referred to the neurology department of our hospital due to suspected Parkinson's disease. The present illness had caused sudden deafness and spinal canal stenosis >10 years earlier, but diabetes mellitus and cardiac disease had not yet developed. Although magnetic resonance imaging, brain perfusion SPECT, and electrocardiography one month before and after ^{123}I-MIBG SPECT yielded unremarkable results, dopamine transporter imaging indicated a severe decrease in bilateral striatum accumulation.

A nuclear medicine physician administered 111 MBq of ^{123}I-MIBG (FUJIFILM RI Pharma, Co., Ltd, Tokyo Japan) by intravenous injection. We acquired planar images with a LMEGP and IQ-SPECT with SZC after 20 min (early phase) and 3 h (delay phase), respectively.

The reconstructed IQ-SPECT image and polar map with NC and ACSC are provided in Fig.8. The heart to mediastinum ratio (HMR) calculated from planar imaging was 3.88 for the early phase and 4.45 for the delayed phase. The short axis image and vertical long axis images with NC and ACSC in the early phase had visually almost the same image quality. However, the %uptake of ACSC image of the inferolateral wall was slightly higher than that of the NC image. Meanwhile, the NC images in the delayed phase revealed a mild low %uptake in the inferior and inferolateral walls, and the %uptake of the NC image was 6.8 – 12.4% lower than that of the ACSC image. The patient was diagnosed with normal MIBG uptake by the consensus of two nuclear medicine physicians.

Discussion

IQ-SPECT imaging using a radiopharmaceutical agent labeled with ^{99m}Tc or ^{201}Tl can be performed with a scan time or administered dose of one-fourth

that of C-SPECT [24, 25]. However, IQ-SPECT using a ^{123}I-labeled radiopharmaceutical agent has not been fully evaluated. The nuclear cardiology imaging of ^{123}I-labeled BMIPP or MIBG is important for the diagnosis of cardiac conditions such as heart failure [2 – 6], unstable angina, vasospastic angina and Takotsubo cardiomyopathy [14 – 16]. C-SPECT with ^{123}I-labeled BMIPP or MIBG leads to patient discomfort and motion due to long scan time; thus, such diagnostic imaging increases the false-positive or false-negative rate due to artifacts. Therefore, the short-term acquisition of myocardial SPECT is very important, and the evaluation of the characteristics for IQ-SPECT compared to those of C-SPECT is of major clinical significance. Hence, we performed basic research using anthropomorphic phantoms.

The defect area of the myocardial phantom was set to the inferior wall. Myocardial defects in the inferior wall yielded the most affected scatter and attenuation, as reported in a previous study [30, 39]. Therefore, we determined that the inferior defect would be most appropriate for evaluating the effects of AC and SC. Furthermore, we did not evaluate SC but only AC. The influence of attenuation and scatter radiation should be simultaneously corrected. However, we performed image assessment of AC images. If ACSC images differ from NC images in image quality, it is not possible to clarify whether the cause of the difference in image quality is AC or SC. Therefore, we added AC images to determine whether the difference in image quality was the effect of AC or SC.

The C-SPECT and IQ-SPECT with NC images of the normal myocardium obtained low visual homogeneity scores due to attenuation artifacts of the inferior and inferolateral walls. However, the visual homogeneity score and %uptake of IQ-SPECT images with NC obtained a higher value than did the C-SPECT images with NC. The attenuation artifacts were improved by AC, and the characteristics were similar to those of IQ-SPECT with ^{99m}Tc and ^{201}Tl images [32]. The ACSC IQ-SPECT image had good homogeneity uptake, whereas the ACSC C-SPECT image achieved a relatively significantly lower

homogeneity score due to a mild decrease in the inferolateral wall. The IQ-SPECT images were obtained with 208° acquisition, while the C-SPECT images were obtained with 360° acquisition. The C-SPECT images with 208° acquisition using a low-energy high-resolution collimator were found to cause the attenuation artifacts in the inferior and inferolateral walls due to missing data of the peripheral right posterior oblique region as well as an acquisition of 180° [40, 41]. Nevertheless, the IQ-SPECT with 208° acquisition had little influence on the attenuation artifacts in comparison to that of C-SPECT with 360° acquisition. We have speculated that this may be associated with the specific shape of the SZC. However, we could not accurately conclude the influence of attenuation artifacts with ^{123}I IQ-SPECT images in our study. The collimator design has an important role in the determination of image quality. In particular, the ^{123}I radiopharmaceuticals require an appropriate collimator in order to enhance the image quality due to the septal penetration and down-scatter occurring by γ-rays of 529 keV [42]. Indeed, the defect detectability of IQ-SPECT was not good compared to that of C-SPECT. We hypothesized that the defect detectability of IQ-SPECT was affected by the scatter radiation from the liver in addition to the down scatter from septal penetration by the SZC. The influence of the septal penetration, down-scatter of 529keV, and scatter radiation from the liver by the SZC has not been fully evaluated. Therefore, future studies should investigate the influence of scatter radiation from the liver and septal penetration of the SZC with ^{123}I radionuclides.

The detectability of IQ-SPECT including defect extent and severity was inferior to that of C-SPECT. However, the defect score of IQ-SPECT images with NC and ACSC met the defect score criteria. Therefore, we conclude that ^{123}I IQ-SPECT that takes advantage of short-term acquisition can be clinically applied. To improve the estimation of the defect extent and severity, the creation of the normal database (NDB) and the image interpretation of combined NC and ACSC images will be beneficial for diagnosis. We have already created a Japanese NDB by gender with ^{99m}Tc and ^{201}Tl IQ-SPECT

images to objectively evaluate the typical myocardial distribution for IQ-SPECT; thus evaluation of the sensitivity, specificity, and accuracy of IQ-SPECT is possible in the same evaluation as those of C-SPECT [32]. Therefore, the NDB with IQ-SPECT of ^{123}I-MIBG and ^{123}I-BMIPP should be created in the next study.

In the clinical example, the %uptake of the NC images for both early and delayed phases was slightly decreased in the inferolateral wall as well as in the phantom study. However, the %uptake of ACSC images was improved in the inferolateral wall, while the uptake in the apex was low, and the IQ-SPECT images with ^{123}I were similar to those with ^{99m}Tc and ^{201}Tl agents. Therefore, IQ-SPECT has a typical myocardial distribution that differs from that of C-SPECT with all myocardial radiopharmaceuticals.

IQ-SPECT using ^{123}I-MIBG is limited in the acquisition of planar imaging. The SZC cannot acquire planar images due to the multi-focal shapes. Hence, the SZC should be changed to a parallel-hole type to acquire planar images. The series of operations including collimator change requires approximately 10 min, which leads to extension of the examination time and an increase in patient discomfort. Anterior planar images must be acquired to calculate the HMR to support the diagnosis such as the risk classification of heart failure, Parkinson's disease and dementia with Lewy bodies [2 – 13]. Likewise, the D-SPECT system developed by Spectrum Dynamics Medical is also unable to acquire planar images. However, the D-SPECT can generate planograms such as planar images from D-SPECT data instead of planar image [43]. Therefore, IQ-SPECT should also be capable of generating new images similar to planar images from IQ-SPECT data to calculate the HMR without a collimator change.

Conclusion

^{123}I IQ-SPECT imaging significantly improved the attenuation artifact compared with C-SPECT imaging. Although the defect detectability of IQ-SPECT was inferior to that of C-SPECT, ^{123}I IQ-SPECT images with NC and

ACSC met the criteria for defect detectability. Finally, ^{123}I IQ-SPECT could be used for routine examinations.

Acknowledgments

The authors thank Ms. Ayumi Niitsuma, RT at Southern TOHOKU Research Institute for Neuroscience for her assistant of image processing and analysis. Furthermore, we would like to thank Editage (www.editage.jp) for English language editing.

Competing interests

K. Nakajima has undertaken a collaborative research work with Siemens Japan (Tokyo, Japan). No other authors report any potential conflicts of interest relevant to this study.

Figure legends

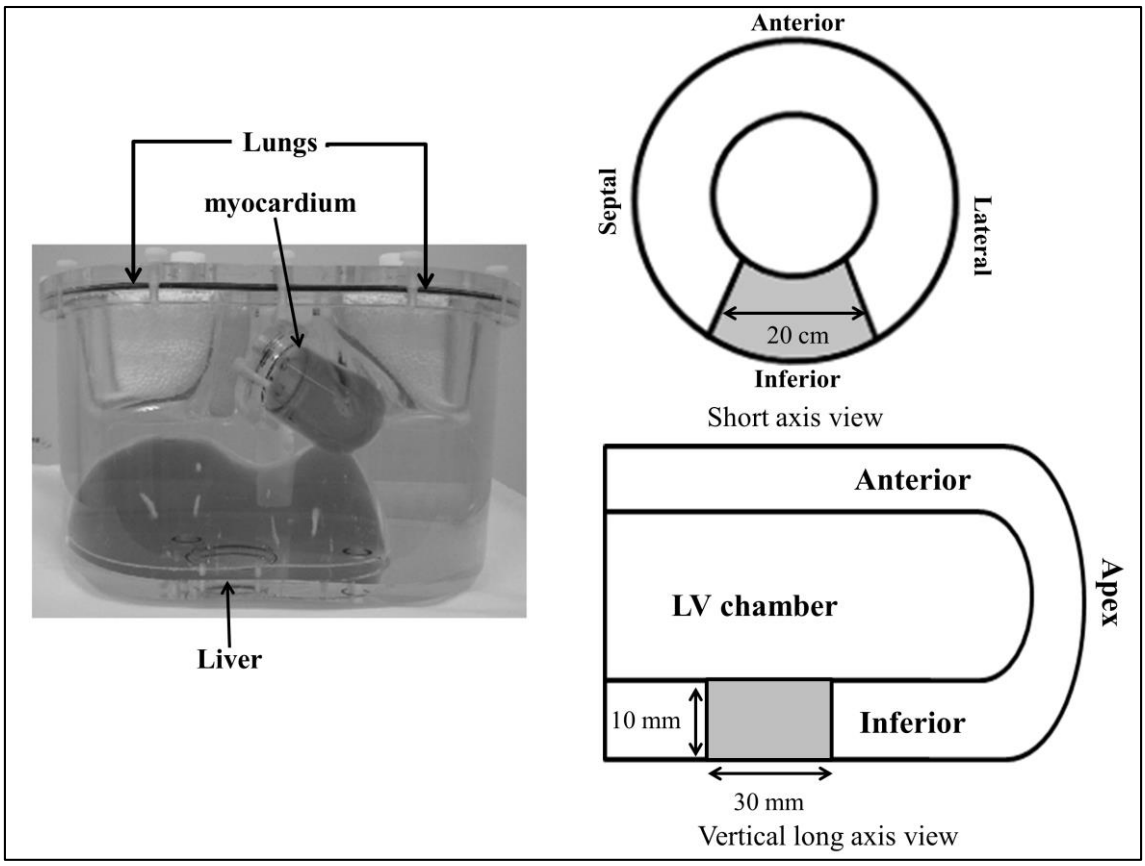

Figure 1. Structure of myocardial phantom with defects. The transmural defect with rectangular shapes was set in the mid to basal inferior position in the LV wall. LV, left ventricular

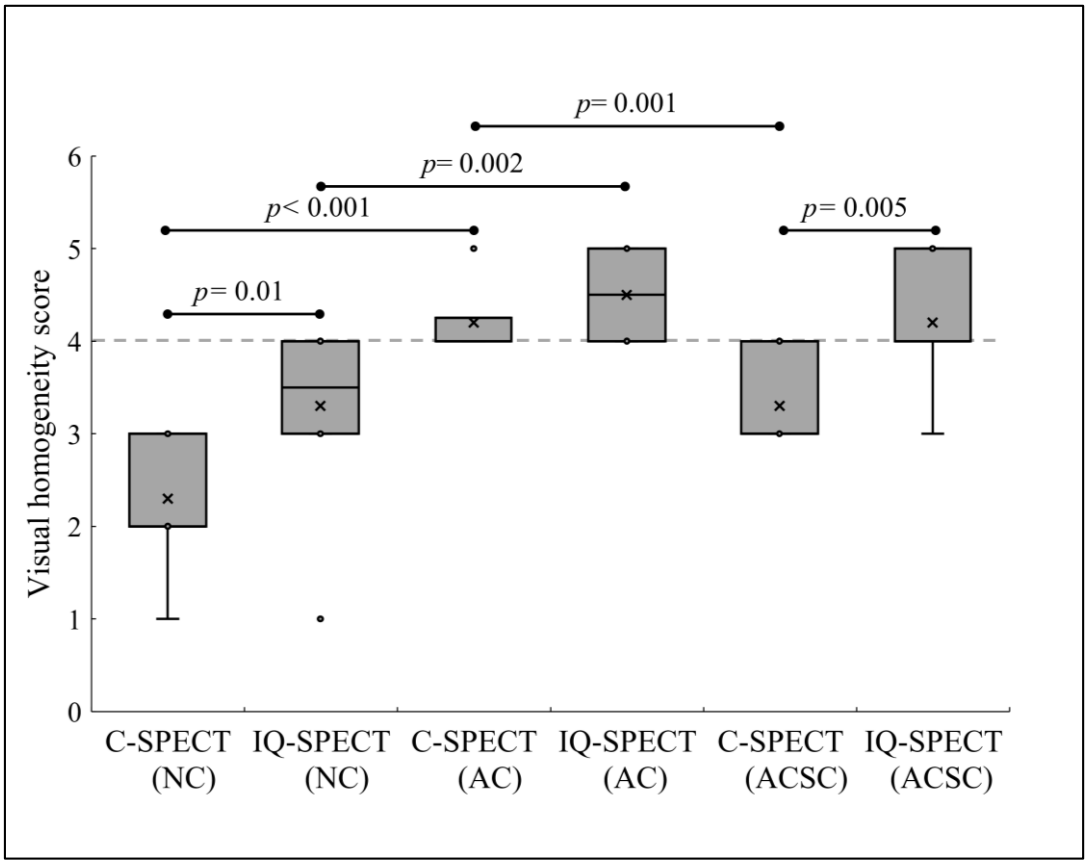

Figure 2. Visual homogeneity score of both conventional SPECT (C-SPECT) and IQ-SPECT for the normal myocardium. NC, no correction; AC, attenuation correction; and ACSC, both attenuation and scatter corrections.

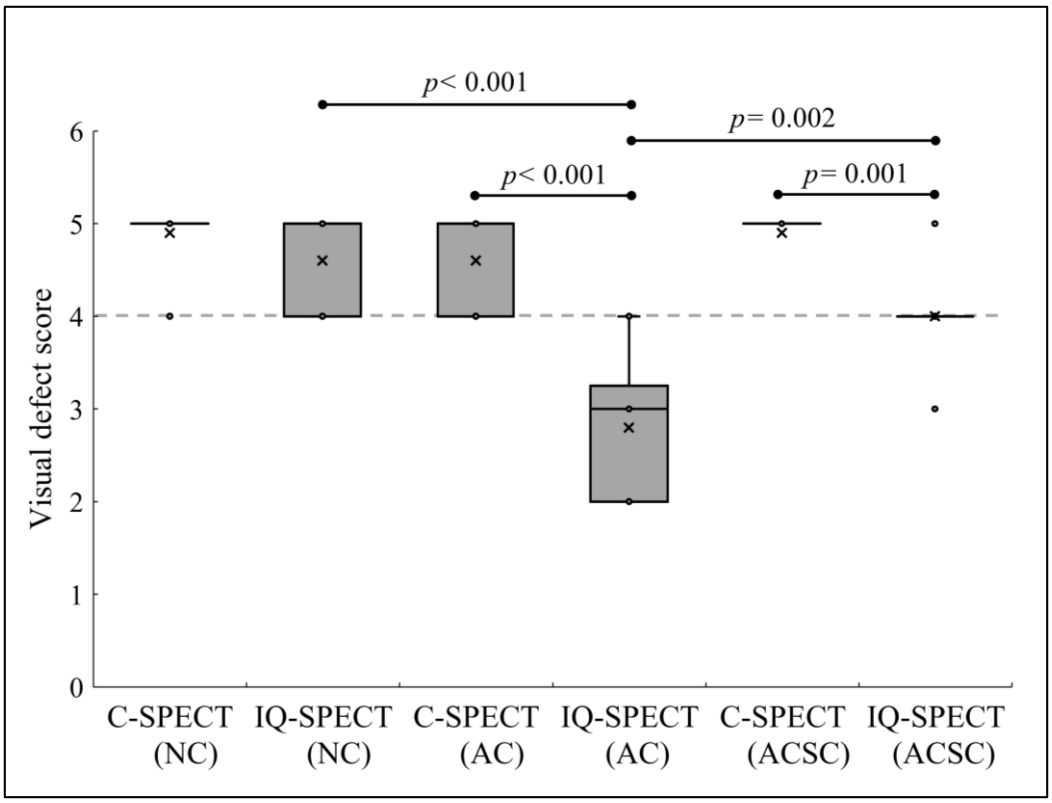

Figure 3. Visual defect score of both conventional SPECT (C-SPECT) and IQ-SPECT for the myocardium with inferior wall defects. NC, no correction; AC, attenuation correction; and ACSC, both attenuation and scatter corrections.

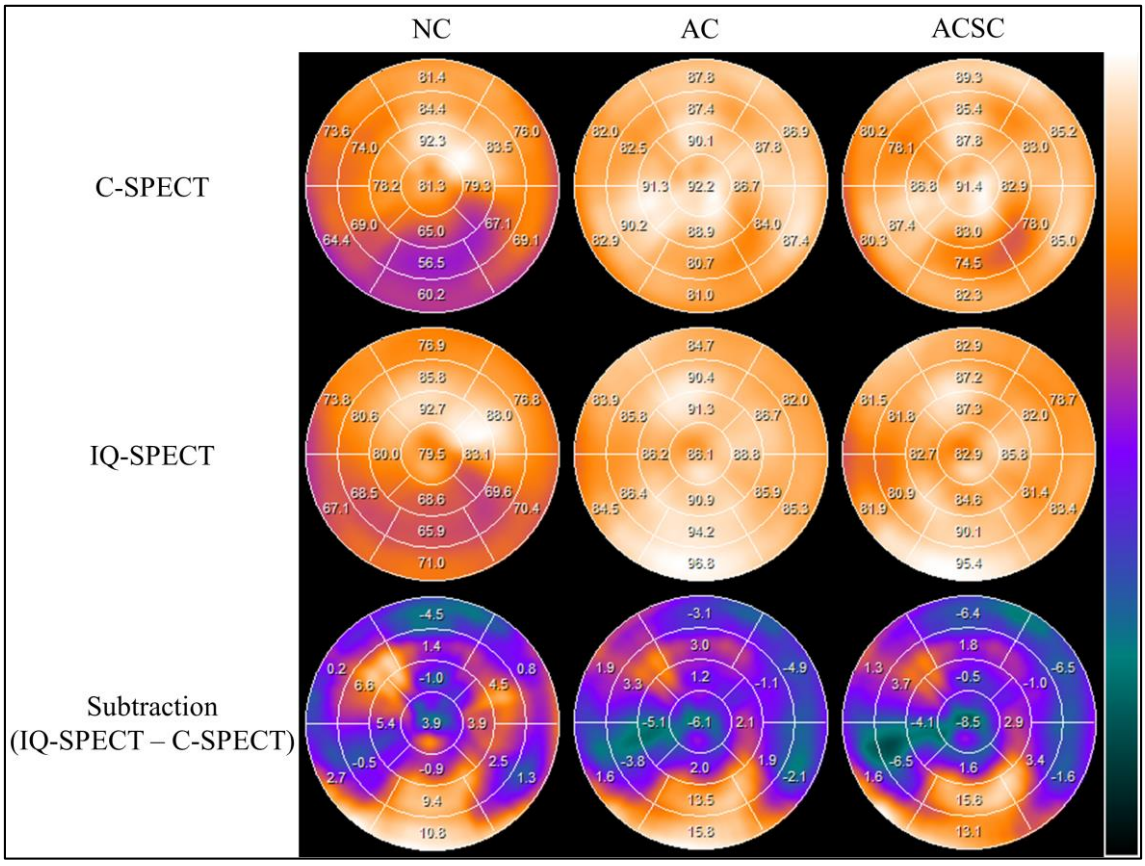

Figure 4. The polar map of conventional SPECT (C-SPECT) and IQ-SPECT for the normal myocardium. NC, no correction; AC, attenuation correction; and ACSC, both attenuation and scatter corrections.

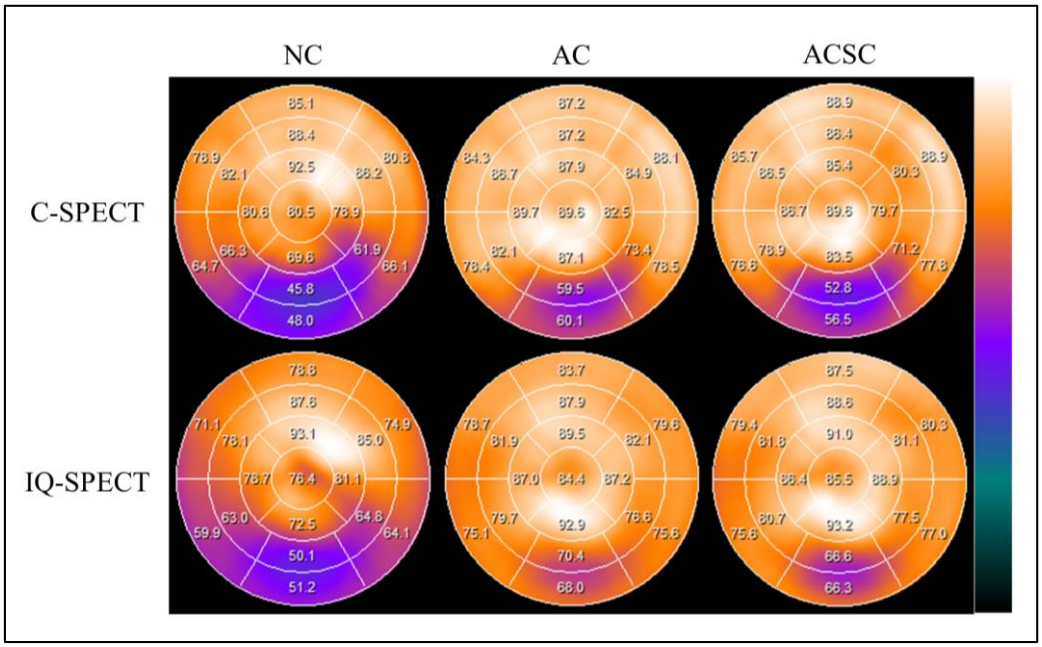

Figure 5. The polar map of conventional SPECT (C-SPECT) and IQ-SPECT for the myocardium with inferior wall defects. NC, no correction; AC, attenuation correction; and ACSC, both attenuation and scatter corrections.

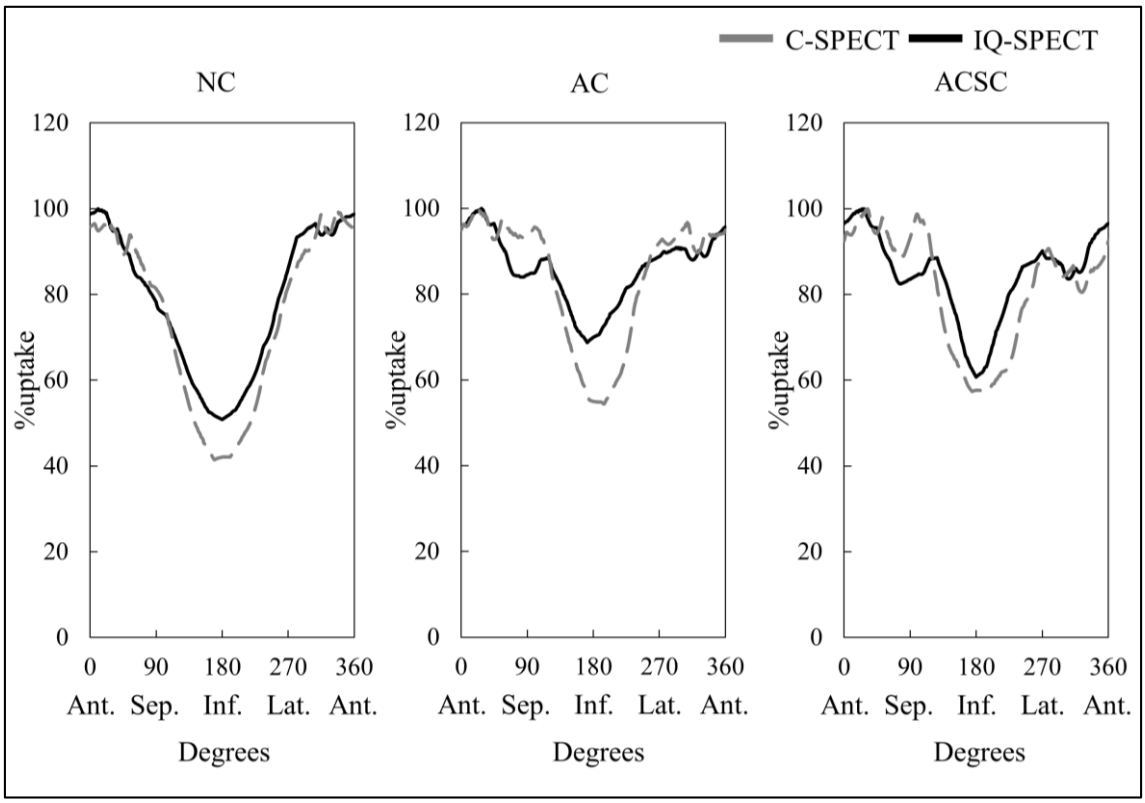

Figure 6. Circumferential count profiles of the short axial image with defect area. NC, no correction; AC, attenuation correction; and ACSC, both attenuation and scatter corrections; Ant., anterior; Sep., septum; Inf., inferior; Lat., lateral.

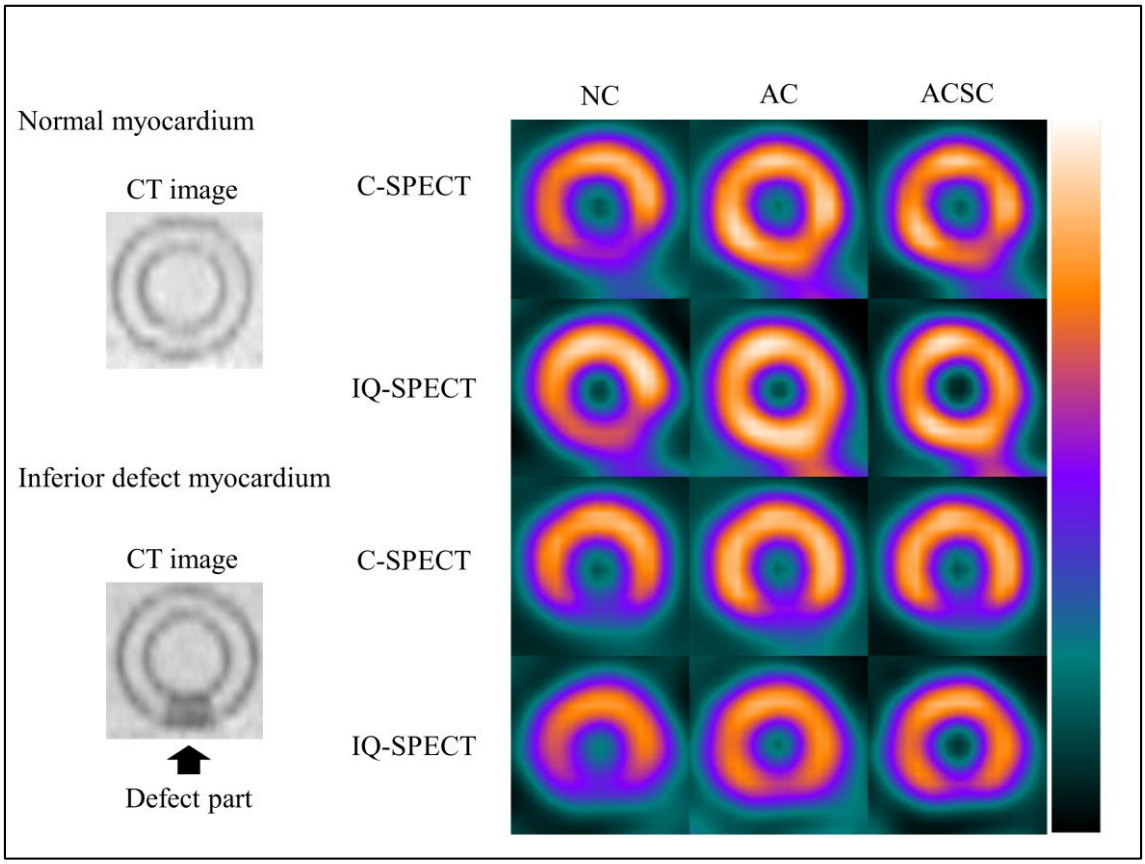

Figure 7. The conventional SPECT (C-SPECT) and IQ-SPECT images with no correction (NC), attenuation correction (AC) and both attenuation and scatter corrections (ACSC) for both myocardial phantoms with normal and the inferior wall defects. Computed tomography (CT) images with normal and inferior defect myocardial phantoms shown as a reference.

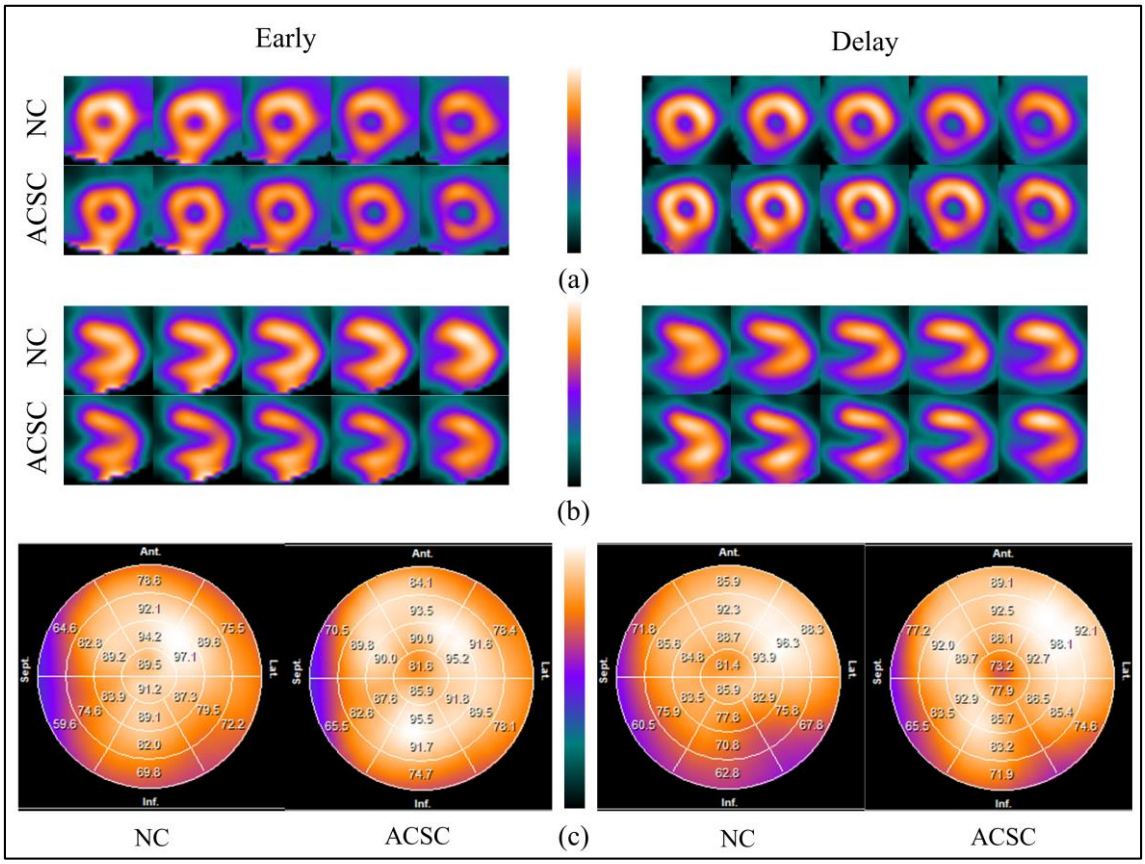

Figure 8. Clinical images and a polar map of early and delay phases for ^{123}I-MIBG with NC and ACSC. The (a), (b) and (c) in the Figure show the short axis image, vertical long axis image and polar map, respectively.

References

1. Matsuo S, Nakajima K, Yamashina S, Sakata K, Momose M, Hashimoto J, et al. Characterization of Japanese standards for myocardial sympathetic and metabolic imaging in comparison with perfusion imaging. Ann Nucl Med. 2009; 23: 517-22.
2. Nakajima K, Nakata T, Matsuo S, Jacobson AF. Creation of mortality risk charts using 123I meta-iodobenzylguanidine heart-to-mediastinum ratio in patients with heart failure: 2- and 5-year risk models. Eur Heart J Cardiovasc Imaging. 2016; 17: 1138-45.
3. Matsuo S, Nakajima K, Nakata T. Prognostic Value of Cardiac Sympathetic Nerve Imaging Using Long-Term Follow-up Data - Ischemic vs. Non-Ischemic Heart Failure Etiology. Circ J. 2016; 80: 435-41.
4. Matsuo S, Nakajima K. Assessment of Cardiac Sympathetic Nerve Function Using 123I- meta- Iodobenzylguanidine Scintigraphy: Technical Aspects and Standardization. Ann Nucl Cardiol. 2015; 1: 27-34.
5. Nakajima K, Nakata T, Yamada T, Yamashina S, Momose M, Kasama S, et al. A prediction model for 5-year cardiac mortality in patients with chronic heart failure using ^{123}I-metaiodobenzylguanidine imaging. Eur J Nucl Med Mol Imaging. 2014; 41: 1673-82.
6. Somsen GA, van Vlies B, de Milliano PA, Borm JJ, van Royen EA, Endert E, et al. Increased myocardial [123I]-metaiodobenzylguanidine uptake after enalapril treatment in patients with chronic heart failure. Heart. 1996; 76: 218-22.
7. Kinbara T, Hayano T, Otani N, Furutani Y, Tanaka S. Iodine-123 metaiodobenzylguanidine imaging can predict future cardiac events in Japanese patients with Parkinson's disease. Ann Nucl Med. 2013; 27: 123-31.
8. Taki J, Yoshita M, Yamada M, Tonami N. Significance of ^{123}I-MIBG scintigraphy as a pathophysiological indicator in the assessment of Parkinson's disease and related disorders: it can be a specific marker for Lewy body disease. Ann Nucl Med. 2004; 18: 453-61.

9. Odagiri H, Baba T, Nishio Y, Iizuka O, Matsuda M, Inoue K, et al. On the Utility of MIBG SPECT/CT in Evaluating Cardiac Sympathetic Dysfunction in Lewy Body Diseases. PLoS One. 2016; 11: e0152746.
10. Yoshita M, Arai H, Arai H, Arai T, Asada T, Fujishiro H, et al. Diagnostic accuracy of 123I-meta-iodobenzylguanidine myocardial scintigraphy in dementia with Lewy bodies: a multicenter study. PLoS One. 2015; 10: e0120540.
11. Sakamoto F, Shiraishi S, Yoshida M, Tomiguchi S, Hirai T, Namimoto T, et al. Diagnosis of dementia with Lewy bodies: diagnostic performance of combined ^{123}I-IMP brain perfusion SPECT and ^{123}I-MIBG myocardial scintigraphy. Ann Nucl Med. 2014; 28: 203-11.
12. Nakajima K, Yoshita M, Matsuo S, Taki J, Kinuya S. Iodine-123-MIBG sympathetic imaging in Lewy-body diseases and related movement disorders. Q J Nucl Med Mol Imaging. 2008; 52: 378-87.
13. Inui Y, Toyama H, Manabe Y, Sato T, Sarai M, Kosaka K, et al. Evaluation of probable or possible dementia with lewy bodies using 123I-IMP brain perfusion SPECT, ^{123}I-MIBG, and ^{99m}Tc-MIBI myocardial SPECT. J Nucl Med. 2007; 48: 1641-50.
14. Takeishi Y, Fujiwara S, Atsumi H, Takahashi K, Sukekawa H, Tomoike H. Iodine-123-BMIPP imaging in unstable angina: a guide for interventional strategy. J Nucl Med. 1997; 38: 1407-11.
15. Nakajima K, Shimizu K, Taki J, Uetani Y, Konishi S, Tonami N, et al. Utility of iodine-123-BMIPP in the diagnosis and follow-up of vasospastic angina. J Nucl Med. 1995; 36: 1934-40.
16. Matsuo S, Nakajima K, Kinuya S, Yamagishi M. Diagnostic utility of ^{123}I-BMIPP imaging in patients with Takotsubo cardiomyopathy. J Cardiol. 2014; 64: 49-56.
17. Cooper JA, Neumann PH, McCandless BK. Effect of patient motion on tomographic myocardial perfusion imaging. J Nucl Med. 1992; 33: 1566-71.

18. Botvinick EH, Zhu YY, O'Connell WJ, Dae MW. A quantitative assessment of patient motion and its effect on myocardial perfusion SPECT images. J Nucl Med. 1993; 34: 303-10.
19. Tanaka H, Chikamori T, Hida S, Uchida K, Igarashi Y, Yokoyama T, et al. Comparison of myocardial perfusion imaging between the new high-speed gamma camera and the standard anger camera. Circ J. 2013; 77: 1009-17.
20. De Lorenzo A, Fonseca LM, Landesmann MC, Lima RS. Comparison between short-acquisition myocardial perfusion SPECT reconstructed with a new algorithm and conventional acquisition with filtered back projection processing. Nucl Med Commun. 2010; 31: 552-7.
21. Caobelli F, Thackeray JT, Soffientini A, Bengel FM, Pizzocaro C, Guerra UP. Feasibility of one-eighth time gated myocardial perfusion SPECT functional imaging using IQ-SPECT. Eur J Nucl Med Mol Imaging. 2015; 42: 1920-8.
22. Caobelli F, Kaiser SR, Thackeray JT, Bengel FM, Chieregato M, Soffientini A, et al. IQ SPECT allows a significant reduction in administered dose and acquisition time for myocardial perfusion imaging: evidence from a phantom study. J Nucl Med. 2014; 55: 2064-70.
23. Zeintl J, Rempel TD, Bhattacharya M, Malmin RE, Vija AH. Performance characteristics of the SMARTZOOM® collimator. Nuclear Science Symposium and Medical Imaging Conference (NSS/MIC) IEEE 2011; 2426-29.
24. Onoguchi M, Konishi T, Shibutani T, Matsuo S, Nakajima K. Technical Aspects: Image Reconstruction. Ann Nucl Cardiol 2016; 2: 68-72.
25. Matsuo S, Nakajima K, Onoguchi M, Wakabayash H, Okuda K, Kinuya S. Nuclear myocardial perfusion imaging using thallium-201 with a novel multifocal collimator SPECT/CT: IQ-SPECT versus conventional protocols in normal subjects. Ann Nucl Med. 2015; 29: 452-9.
26. Onishi H, Matsutomo N, Kangai Y, Saho T, Amijima H. Differential impact of multi-focus fan beam collimation with L-mode and conventional

systems on the accuracy of myocardial perfusion imaging: Quantitative evaluation using phantoms. Asia Ocean J Nucl Med Biol. 2013; 1: 28-34.

27. Havel M, Kolacek M, Kaminek M, Dedek V, Kraft O, Sirucek P. Myocardial perfusion imaging parameters: IQ-SPECT and conventional SPET system comparison. Hell J Nucl Med. 2014; 17: 200-3.
28. Shibutani T, Onoguchi M, Funayama R, Nakajima K, Matsuo S, Yoneyama H, et al. The Optimal Reconstruction Parameters by Scatter and Attenuation Corrections Using Multi-focus Collimator System in Thallium-201 Myocardial Perfusion SPECT Study. Nihon Hoshasen Gijutsu Gakkai Zasshi. 2015; 71: 1103-12.
29. Okuda K, Nakajima K, Matsuo S, Kondo C, Sarai M, Horiguchi Y, et al. Creation and characterization of normal myocardial perfusion imaging databases using the IQ·SPECT system. J Nucl Cardiol. 2017 Jan 3. doi: 10.1007/s12350-016-0770-2.
30. Shibutani T, Onoguchi M, Yoneyama H, Konishi T, Matsuo S, Nakajima K, et al. Characteristics of single- and dual-photopeak energy window acquisitions with thallium-201 IQ-SPECT/CT system. Ann Nucl Med. 2017; 31: 529-35.
31. Yoneyama H, Shibutani T, Konishi T, Mizutani A, Hashimoto R, Onoguchi M, et al. Validation of the left ventricular ejection fraction and quantitation of myocardial abnormality with IQ-SPECT system in small-heart patients. J Nucl Med Technol. 2017; 45: 201-7.
32. Nakajima K, Okuda K, Momose M, Matsuo S, Kondo C, Sarai M, et al. IQ·SPECT technology and its clinical applications using multicenter normal databases. Ann Nucl Med 2017; 31: 649-59.
33. Hippeläinen E, Mäkelä T, Kaasalainen T, Kaleva E. Ejection fraction in myocardial perfusion imaging assessed with a dynamic phantom: comparison between IQ-SPECT and LEHR. EJNMMI Phys. 2017; 4: 20.
34. Du Y, Bhattacharya M, Frey EC. Simultaneous Tc-99m/I-123 dual-radionuclide myocardial perfusion/innervation imaging using Siemens

IQ-SPECT with SMARTZOOM collimator. Phys Med Biol. 2014; 59: 2813-28.

35. Inoue Y, Shirouzu I, Machida T, Yoshizawa Y, Akita F, Minami M, et al. Collimator choice in cardiac SPECT with I-123-labeled tracers. J Nucl Cardiol. 2004; 11: 433-9.
36. Zeintl J, Vija AH, Yahil A, Hornegger J, Kuwert T. Quantitative accuracy of clinical ^{99m}Tc SPECT/CT using ordered-subset expectation maximization with 3-dimensional resolution recovery, attenuation, and scatter correction. J Nucl Med. 2010; 51: 921-8.
37. Okuda K, Nakajima K, Yamada M, Wakabayashi H, Ichikawa H, Arai H, et al. Optimization of iterative reconstruction parameters with attenuation correction, scatter correction and resolution recovery in myocardial perfusion SPECT/CT. Ann Nucl Med. 2014; 28: 60-8.
38. Christian TF, Schwartz RS, Gibbons RJ. Determinants of infarct size in reperfusion therapy for acute myocardial infarction. Circulation. 1992; 86: 81-90.
39. Shibutani T, Onoguchi M, Yamada T, Kamida H, Kunishita K, Hayashi Y, et al. Optimization of the filter parameters in (99m)Tc myocardial perfusion SPECT studies: the formulation of flowchart. Australas Phys Eng Sci Med. 2016; 39: 571-81.
40. Tamaki N, Mukai T, Ishii Y, Fujita T, Yamamoto K, Minato K, et al. Comparative study of thallium emission myocardial tomography with 180 degrees and 360 degrees data collection. J Nucl Med. 1982; 23: 661-6.
41. Nakajima K, Okuda K, Kawano M, Matsuo S, Slomka P, Germano G, et al. The importance of population-specific normal database for quantification of myocardial ischemia: comparison between Japanese 360 and 180-degree databases and a US database. J Nucl Cardiol. 2009; 16: 422-30.
42. Dobbeleir AA, Hambÿe AS, Franken PR. Influence of high-energy photons on the spectrum of iodine-123 with low- and medium-energy collimators:

consequences for imaging with 123I-labelled compounds in clinical practice. Eur J Nucl Med. 1999; 26: 655-8.

43. Nakajima K, Okuda K, Yokoyama K, Yoneyama T, Tsuji S, Oda H, et al. Cross calibration of 123I-meta-iodobenzylguanidine heart-to-mediastinum ratio with D-SPECT planogram and Anger camera. Ann Nucl Med. 2017; 31: 605-15.